Classic and Topologic Dimensional Effects in SnO2 Thin Films Detected by Surface Plasmon Resonance Technique

Article *in* Journal of Nanomaterials & Molecular Nanotechnology · January 2013

DOI: 10.41172/2324-8777.1000114

CITATIONS
0

READS
28

8 authors, including:

Viktor Grinevich
Odessa National University
57 PUBLICATIONS **55** CITATIONS
SEE PROFILE

Liudmila M. Filevska
Odessa National University
47 PUBLICATIONS **51** CITATIONS
SEE PROFILE

Oleg Mischuk
National Academy of Sciences of Ukraine
12 PUBLICATIONS **25** CITATIONS
SEE PROFILE

S. P. Rudenko
National Academy of Sciences of Ukraine
43 PUBLICATIONS **157** CITATIONS
SEE PROFILE

Grinevich et al., J Nanomater Mol Nanotechnol 2013, 2:3
http://dx.doi.org/10.4172/2324-8777.1000114

Journal of Nanomaterials & Molecular Nanotechnology

Research Article

A SCITECHNOL JOURNAL

Classic and Topologic Dimensional Effects in SnO_2 Thin Films Detected by Surface Plasmon Resonance Technique

Grinevich VS[1*], Filevskaya LN[1], Maximenko LS[2], Matyash IE[2], Mischuk ON[2], Rudenko SP[2], Serdega BK[2] and Smyntyna VA[1]

Abstract

Internal reflection features caused by the surface plasmon resonance in nanoscale films containing defect tin dioxide clusters in the stoichiometric dielectric matrix are studied by means of polarization modulation of electromagnetic radiation. The angular and spectral characteristics of reflectances R_s^2 and R_p^2 of *s*- and *p*-polarized radiation and their polarization difference $\rho=R_s^2-R_p^2$ are measured in the wavelength range λ=400-1600 nm. The obtained experimental characteristics ρ(θ, λ) (θ is the radiation incidence angle) represent the optical property features associated with the film structure and morphology. Surface plasmon polaritons and local plasmons excited by *s*- and *p*-polarized radiation are detected; their frequency and relaxation properties are determined. The technique employed for studying surface plasmon resonance in tin dioxide films is appeared to be structurally sensitive.

Keywords

Tin dioxide; Thin film; Surface Plasmon resonance

Introduction

The urgency of developing and studying new nanoscale materials is caused both by fundamental interest in their properties, and their potential applicability in solid-state electronics. The study of nanoscale tin oxide (SnO_2), in particular, is motivated by its numerous applications as transparent electrode materials, gas sensors, and catalysts in oxidation processes [1]. The list of these nanostructures applications should also be complemented by the possibility of controlling light fluxes in materials in which surface plasmon resonance (SPR) effects are observed.

The SPR phenomena properties are enough effective for the investigation of the nanostructured materials. Such investigations objects are clustered films, which are the media where classic and topologic dimension effects display themselves. Therefore, the correlation established by means of SPR between morphology and optical parameters of composite heterosystems, which contain metallic and dielectric components seems preferable in comparison with other methods. The basis for such understanding is the property of a resonance in general, and SPR in particular, so far as it has more intensive dispersion of it's parameters in the vicinity of the basic frequency, and hence, it has more detective ability relatively to dielectric properties of the films.

A working model of this study object (tin dioxide film) was proposed taking into account its surface specificity caused by dual Sn valence. Precisely, this feature provides reversible transformations of the SnO_2 surface composition from stoichiometric Sn^{4+} to reduced Sn^{2+}, depending on the chemical potential of oxygen of the system [1]. Surface reduction modifies its electronic structure and leads to the formation of deep electron levels in the band gap. This provides a decrease in the electron work function, the presence of free carriers in a material, and hence, the possibility of observing the SPR phenomenon.

Recently, the method for studying materials has become widespread, whose informative power is amplified by the properties SPR. It is generally believed that the SPR phenomenon is mostly characteristic for such metals as silver, gold, aluminium, and copper, whose permittivity becomes negative (the refractive index is less than unity) in the visible spectral region [2,3]. This is the case when this phenomenon is observed by measuring the reflectance using one of the widespread optical schemes, i.e. the Otto [4], or Kretschmann geometry [5].

However, as shown recently [6], the SPR phenomenon can be observed even in the case when it is weakly detected in comparison with conventional methods. It is reported a relatively new method for measuring optically anisotropic effects, which is based on polarization modulation (PM) of electromagnetic radiation [7]. One version of this method introduces a parameter called the polarization difference $\rho=R_s^2-R_p^2$ of reflectances of radiation, which wave electric-field vectors are perpendicular or parallel to the incidence plane (optical axis), respectively. The increased detection and information ability of this parameter were multiply demonstrated in studying various effects of amplitude and phase anisotropy [6,8].

It is well known that the reflection conditions (including internal) being most convenient for SPR measurements according to Fresnel formulas [9], heavily depend on the electromagnetic wave polarization state. These two factors stimulate application of the PM method to study nanoscale cluster films of tin dioxide. In contrast to nanoscale metal films, a feature of such objects is that their properties are controlled not only by the sample surface state, but also by their bulk features. Therefore, it can be expected that the PM method will become an informative complement to such a widely used method of studying nanoscale objects as atomic-force microscopy.

The PM method introduces the polarization difference ρ(θ, λ, *d*, …) parameter, where (θ, λ, and *d* are the incidence angle of light, wavelength, and film thickness, respectively, etc.), which has multivalued forms. They contain information both on the optical properties of studied objects, and on their morphology and structure.

In this case, there are certain advantages in using films consisting of isolated or contacting particles in comparison with continuous films. In particular, the restriction associated with the difference of wave vectors at the interaction of light and plasmon excitation

***Corresponding author:** Grinevich VS, Odessa Mechnikov National University, ul. Dvoryanskaya 2, Odessa, 65082, Ukraine, E-mail: grinevich@onu.edu.ua

Received: February 22, 2013 **Accepted:** April 17, 2013 **Published:** April 26, 2013

in films is cancelled for contacting particles due to the presence of surface curvature [10]. Furthermore, this restriction, as it was shown previously [8], is also lifted for the initial state of light polarization because not only *p*-polarized, but also *s*-polarized radiation may excite SPR in the cluster film.

The SPR studies in nanocomposite films as Al, Au, and ITO metal clusters in the dielectric matrix of WO_3, SnO_2, and TiO_2 oxide materials are well known [11]. In this study, nanostructured tin oxide films are considered as nanocomposites containing clusters of defect nonstoichiometric tin oxide (SnO_x), in the dielectric matrix of stoichiometric SnO_2.

Thus, the aim of this study is interpretation of the variety of the films' properties, using SPR experimental data obtained by the polarization modulation technique.

Experimental Procedure

Two type's samples of tin dioxide, obtained by means of two principally different technologies, were used for the experiments. The first type samples were prepared by the technique described in detail [12]. This technique contained the following basic stages: preparation of an acetone solution of polymer (PVA), preparation of an acetone solution of the SnO_2 precursor, mixing of these two solutions, covering of a substrate by the rotational method using centrifuging (spin-coating), drying, and annealing. Bis(acetylacetonato)dichlorotin (BADCT) complex was used as a tin dioxide precursor. A cover glass 22×22 mm was used as a substrate. Samples were kept at room temperature for 15 min to remove acetone, and were then annealed in air at 600°C for 6 h for thermal decomposition of organic components (BADCT and PVA), and subsequent removal of their decay products. After the annealing, tin dioxide formed due to BADCT thermal decomposition remained on a substrate, which was confirmed by our thermogravimetric studies of this precursor [13]. PVA was used to structurize the film, at the stage of solution preparation and the substrate covering.

The main samples' parameters are given in the Table 1. The average films' thickness data for the studied area surface (1×1) μm was obtained by atomic-force microscopy (AFM), with an error no more than 2%.

The inset to Figure 1 shows the sample T4.R1 phase topology of 1000×1000 nm surface, obtained using the commercial Nanoscope IIIa (Digital Instruments, USA) atomic-force microscope. The histogram of the probabilistic films' sizes composition, obtained by Fourier analyses of the surface profile, is shown in Figure 1 by the solid curve. Histograms approximated by Gaussian functions show that the film consists of two groups of clusters within the histogram areas. One of them covers the range of 50-200 nm with an extremum at 137 nm; the other, with an extremum at 310 nm occupies the range of 200-500 nm. One may notice that the visual evaluation of the film compared with its quantitative characteristic allows concluding that large clusters are the isolated conglomerates, consisting of smaller ones separated by nanoscale spacing of thermal origin. Below it will be shown that this structural feature of the films influences their spectral characteristics shapes. The identified cluster structure of the films with numerous defects (crystallite–cluster interfaces) causes formation of electron plasma in them.

The second type of the samples were films, nanosized along their thickness dimension and prepared in air atmosphere, by means of reactive spaying [14] of water solution of $SnCl_4$, on the glass substrate heated to 450°C. The $SbCl_5$ solution was used as a doping, which provides the increasing of electro conductivity up to the values of σ=10-50 $Om^{-1} cm^{-1}$. According to the phase topology obtained from the AFM data of the samples, the films had 110 nm thicknesses and consisted of the inter-contacting clusters with insignificant spread in sizes.

Table 1: The principal parameters of the samples: thickness and the content of the main components in the initial solution.

Sample Type	*d*, nm	BADCT content in the initial solution, %	PVA content in the initial solution, %
T4.R1	230-400	4	1
T4.R0.5	420	4	0.5
T2.R0.1	350	2	0.1
T2.R2	160	2	2
T0.5R0.1	80-100	0.5	0.1

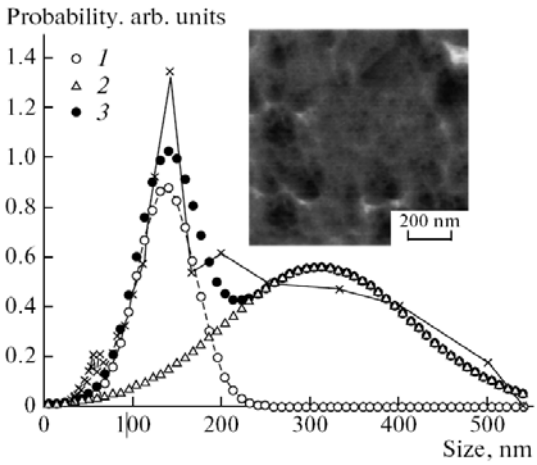

Figure 1: Histogram of the probabilistic-size composition of sample T4.R1: the Fourier spectrum of the surface profile (solid curve) (*1*,*2*) expanded in Gaussian curves and (*3*) their sum. The inset shows the AFM phase topology.

The samples were placed on the reflecting surface of a total internal reflection semicylinder made of melted quartzK with refractive index N_0=1.45, resulted in the critical angle θ_{cr}=42°. The radiation source was an incandescent lamp and a monochromator, with an Ahrens prism at the output slit. The internal reflection coefficients, R_s^2 and R_p^2 of radiation polarized perpendicular and parallel (*s*- and *p*-polarizations, respectively), relatively to the light incidence plane both with their polarization difference $\rho=R_s^2-R_p^2$ were measured considering the light incidence angle in one case, and the wavelength in the range of λ=400-1600 nm in the other.

Their measurements were performed using PM. Figure 2 shows a possible version of the optical scheme with polarization modulation for measuring both the characteristics of internal reflection and the reflection coefficient difference for the *s* and *p* polarizations. An MDR-4 monochromator with a KGM-150 halogen lamp at the input and a polarizer at the output were used as sources of linearly polarized light. The monochromator's light wavelength varied in the range 0.4–2 μm, with an intensity not lower than10^{12} photons $cm^2 s^{-1}$ at a slit width of 0.1 mm. The direction of linearly polarized light has an angle

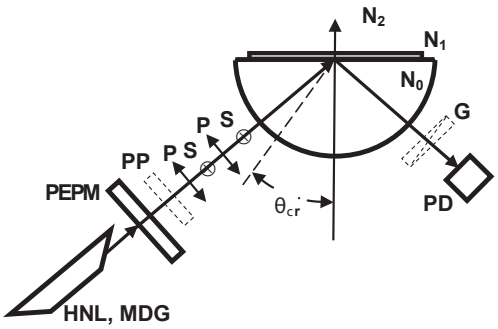

Figure 2: Optical scheme of the experimental setup for measuring the angular characteristics of the polarization difference ρ by means of polarization modulation: (HNL, MDG) helium-neon laser or monochromator; (PP) quarter-wave phase plate; (PEM) photoelastic polarization modulator; (*p*, *s*) linear polarizations, whose azimuths are parallel and perpendicular to the plane of incidence; (G) Glan prism, (PD) photodetector; (φ_{cr}) critical angle of total internal reflection; and (N_0, N_1, N_2) refractive indices of glass, metal, and air, respectively.

of 45° with the modulator axes. The polarization modulator PEM [7] is a dynamic phase plate, which can controllably operate in two modes. In the first mode, it operates as a half-wave plate, changing the azimuth of a linearly polarized wave from parallel to perpendicular relatively the light plane of both incidences twice for the modulation period. In the second mode, operating as a quarter-wave plate, the modulator transforms the linear polarization into circular one once for the period. In this case, a stationary quarter-wave phase plate was installed after the PEM to transform linearly polarized light into orthogonal once for the period. This version was preferred in using a photodetector with a reduced sensitivity at the doubled modulation frequency. In both cases, the modulator rotated round the optical axes of the measuring system, so that the polarization azimuths of light were successively parallel and perpendicular to the incidence plane (*p* and *s* polarizations, respectively). After interaction both with the prism (melted quartz) and the film sensitive to resonance, the light was directed to the photodetector PD (silicon or germanium photodiode), which generated a signal having a variable component. In the first case, it has the frequency equal to the doubled modulation frequency and to the modulation frequency itself in the second case. This component is proportional to the reflection coefficient difference for the *p* and *s* polarizations. In this case, the modulation frequency was so low (50 kHz), that it did not resulted in the electromagnetic wave frequency.

Since the reflection coefficients R_p^2 and R_s^2 are different, the signal from the photodetector PD, measured by a selective voltmeter at the modulation frequency, is proportional to the difference of *s*- and *p*-functions, with wavelength (energy) as arguments and light reflection angle:

$$U= [R_s^2(\lambda,\theta)-R_p^2(\lambda,\theta)] \sin\omega t.$$

The applicability of the proposed technique is proved by the fact that the result is the physical difference of two values, produced by the device itself, contrary to the mathematical subtraction where errors are added up and may exceed the subtraction result. Therefore, it is reliable even when the difference signal is lower than the noise of each of them. It is especially important in the case of the long-term instability, accompanying independent measurements.

The linear polarizer employed in the optical scheme allowed measuring the reflection coefficients R_s^2 and R_p^2. For this aim, the polarizer was placed behind the modulator, so that its axis would in turn coincide with the semicylinder axis, and be perpendicular to it in the other case. The polarizer played the role of a "window", which provides an alternating signal for the photodetector variably transmitting light of a certain polarisation. The results of s- or *p*-polarization were measured for radiation reflection from a clean reflecting surface of semicylinder, in the range of angles smaller than the critical, $\theta<\theta_{cr}$. According to the Fresnel formulas, this radiation satisfies the condition $R_s^2>R_p^2$ in the range of angles smaller than the critical, $\theta<\theta_{cr.}$.

It is noteworthy that the measured reflectances correlate with the radiation intensity, and their magnitudes are always positive. However, parameter ρ, depending on the relation of its components, may be negative, ρ<0. Below it will be shown, for "anomalous" reflection at $R_s^2<R_p^2$, which appears in the range of angles larger than the critical one θ_{cr}. Since measurements were carried out by means of a phase-sensitive lock-in- nanovoltmeter, the sign of parameter ρ was calibrated according to $R_s^2>R_p^2$, obtained by reflection from the clean semicylinder surface. This may be carried out by setting the corresponding phase of the reference signal in the measuring device, thus obtaining the alternating voltage of the polarization modulator.

Results and Discussion

The results will be discussed in terms of Fresnel formulas [15], describing the reflection coefficients R_s^2 and R_p^2 dependence, hence, the polarization difference ρ dependence on the light incidence angle θ. The evolution of the polarized light passing through the layers and reflecting from the interfaces is presented in the matrix form. The matrix product, obtained due to the sequence of light transmission, describes the polarization state of light in the final form as

$$M_j=I_{j01}*L_1*I_{j12},$$

Where j=s, p,

$$I_{j01}=\begin{vmatrix}1 & r_{j01}\\ r_{j01} & 1\end{vmatrix},\ I_{j12}=\begin{vmatrix}1 & r_{j12}\\ r_{j12} & 1\end{vmatrix},\ L_1=\begin{vmatrix}\exp(-i\beta) & 0\\ 0 & \exp(i\beta)\end{vmatrix},$$

$$r_{p01}=\frac{N_1\cos(\varphi_0)-N_0\cos(\varphi_1)}{N_1\cos(\varphi_0)+N_0\cos(\varphi_1)},\ r_{p12}=\frac{N_2\cos(\varphi_1)-N_1\cos(\varphi_2)}{N_2\cos(\varphi_1)+N_1\cos(\varphi_2)},$$

$$r_{s01}=\frac{N_0\cos(\varphi_0)-N_1\cos(\varphi_1)}{N_0\cos(\varphi_0)+N_1\cos(\varphi_1)},\ r_{s12}=\frac{N_1\cos(\varphi_1)-N_2\cos(\varphi_2)}{N_1\cos(\varphi_1)+N_2\cos(\varphi_2)},$$

φ_0, φ_1, and φ_2 are the angles of light propagation in the glass, film, and air, respectively:

$$\varphi_1=\arcsin[(N_0\sin\varphi_0)/N_1],\qquad \varphi_2=\arcsin[(N_0\sin\varphi_0)/N_2],$$

And N_0, N_1, and N_2 are the refractive indices of the prism, film, and external medium (air), respectively.

The phase factor

$$\beta=2\pi d_1\sqrt{N_1^2-N_0^2(\sin\varphi_0)^2}\ /\ \lambda$$

is common for both polarizations.

The expressions determine the reflection coefficients for electromagnetic waves of both polarizations:

$R_p=M_{p(2,1)}/M_{p(1,1)}$, $R_s=M_{s(2,1)}/M_{s(1,1)}$,

where $M_{p(2,1)}$, $M_{p(1,1)}$, $M_{s(2,1)}$ and $M_{s(1,1)}$ are the corresponding matrix elements for the *s* and *p* polarizations. And, the expression for the measured difference of the reflection coefficients for the *s* and *p* polarizations will be in the form

$\rho=R_s^2-R_p^2$.

In this case, the cluster film is considered to be planar and homogeneous with effective optical parameters. This supposition is based on the results of AFM studies, which showed that the film surface is smooth with roughness insignificant relatively to the thickness. The structural heterogeneity, nevertheless, is not an obstacle for the characterization of samples' dielectric properties by effective optical parameters due to the clusters' dimensions inproportionality with the wavelengths used.

The experimental results, i.e. the reflection coefficients R_s^2 and R_p^2 and their polarization difference ρ dependencies on the light incidence angle, are shown in Figure 3 for sample T4.R1, in comparison with the calculation result. The choice of the wavelength λ=500 nm will be understood later. The characteristic feature of SPR in metal homogeneous films of optimal thickness is, by definition, a fall in the function R_p^2 (θ), narrow in angular coordinate and deep in amplitude.

The features of SPR, Figure 3 are specific not only for R_p^2 (θ), but also for the R_s^2 (θ) curve, which in the angular range above the critical one, $\theta>\theta_{cr}=42^\circ$, contains the mentioned reflectance slope. This slope is more extended in comparison with the similar metal film's characteristic, which are uniform in thickness, thus does not contradicting the SPR phenomenon in spherical or close-to-spherical objects [10]. The reason is that the light incidence angle should not be measured relatively film surface, but relatively the plane tangent to a cluster surface, hence, arranged at a certain angle to the film plane.

The refractive indices (*n*) and absorbance (*k*) of tin dioxide cluster films in dielectrics, which are necessary to calculate the coefficients R_s^2, R_p^2, and the parameter ρ were determined by means of multiparameter fitting of the calculated curves to the experimental ones. Agreement of these data was achieved due to the artificial approach, i.e. the use of modified Fresnel formulas. The physical nature of the modification is based on the fact that an *s*-polarized wave for the cluster film (in contrast to a homogeneous one), contains a field component oriented in general, along the normal to the cluster surface. Formally it was considered by using different samples thicknesses (d_s, d_p) in the wave field directions having orthogonal polarizations. The applicability of such an approximation does not contradict the structural anisotropy idea discussed [9]. It is evident that an increase in the number of fitting parameters by adding one more unknown complicates the matching process. However, experiment shows that variation range of parameters was limited to 0, 2. Therefore, as the film thickness was known, fitting by selection of refractive indices and absorbance in a limited range was not complicated.

The determined values of the optical constants are in logical agreement with the data [16]. As to the observed disagreement in angular dependences, it should be noted that the film is slightly cuneal and inhomogeneous within the light spot area, whose size increases with angle. Furthermore, in general, the geometrical shape of clusters is not spherical, which would be reflected by an additional condition. Nevertheless, the observed agreement of calculated and measured data in Figure 3 is more than satisfactory.

Furthermore, an unusual conclusion may follows from Figure 3: the SPR phenomenon in metal–dielectric cluster films can also be detected in the case of surface plasmon excitation by unpolarized radiation. It is easy to verify that the above-mentioned shape of clusters leads to resonant interaction of radiation with their electron system not only for *p*-polarized radiation, as in the case of continuous homogeneous metal films, but also for *s*-polarization. Moreover, if the amplitudes of the extrema for corresponding polarization reflect the intensities of the resonant interaction, as it follows from the inequality of the reflectances in the resonance region, $R_{S|SP}^2>R_{P|SP}^2$ (inset to Figure 3), then the shape of clusters, and/or their dielectric stoichiometric environment, is more preferable for SPR of *s*-polarization. Formally, these circumstances are described by the phase synchronism condition [3],

$$\sqrt{\varepsilon_0}\sin\theta_{SP}=\sqrt{\frac{\varepsilon_2\varepsilon_1(\omega)}{\varepsilon_2+\varepsilon_1(\omega)}} \quad (1)$$

following from the equality of wave vectors of excitation and plasmon waves. Here ε_0, $\varepsilon_1(\omega)$, and ε_2 are the real parts of the complex permittivities of the prism, metal film and external medium materials, respectively. Equation (1) expresses the equality of two values: the projection on the metal film of the wave vector $\mathbf{k}_0$ (left-hand side) of radiation propagating in the prism at the resonance angle θ_{sp} and the vector $\mathbf{k}_{sp}$ of the plasmon wave propagating along the surface. In the relation (1) one of its parameters, i.e. θ_{sp}, being an argument of the function ρ(θ), illustrates the possibility of exciting a surface plasmon wave in a wide angular range due to the non-planar cluster surface.

The resonant type of interaction is also evidenced by the spectral characteristics of the parameter ρ(λ) (Figure 4), for samples differing

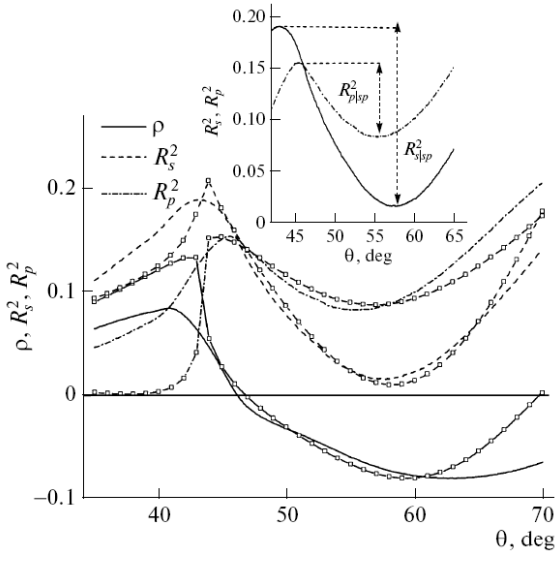

Figure 3: Experimental (curves) angular dependences of the internal reflectances R_S^2(θ), R_P^2(θ) and the parameter ρ(θ) in sample T4.R1 in comparison with calculated (dots) characteristics. The calculation is performed for the following parameters: λ=500 nm, *n*=1.61, *k*=0.1, d_p=290 nm, and d_s=300 nm. The inset shows the different degrees of resonant interaction characterized by the values of $R_{S|SP}^2$ and $R_{P|SP}^2$ in sample T4.R1.

in tin dioxide thickness and its concentration. For three dependences, the negative sign of the relation $\rho=R_s^2-R_p^2$ corresponds to actually measured quantities. From Figure 4a, it becomes clear the choice of the wavelength of 500 nm for the angular dependence of parameter $\rho(\theta)$, shown in Figure 3 for sample T4.R1. It is seen that the curves $\rho(\lambda)$ in the wavelength range λ=400-500 nm contain an extremum for all samples. In this case, the negative sign of characteristics indicates the satisfying of the relation $R_s^2<R_p^2$, hence, confirms surface plasmon excitation by *s*- and *p*- polarized radiation, which is consistent with the angular dependences (Figure 3) of both R_s^2 and R_p^2 and their polarization difference.

Moreover, the magnitude and sign of the parameter ρ and extrema positions of curves have a correlation with the sample thickness and the SnO_2 precursor content in initial solutions. Comparison of samples' parameters with the value and sign of the polarization difference ρ shows that the SnO_2 precursor content growth results in a decrease in parameter ρ amplitude, along the vertical axis. It is noteworthy that the data for sample T2. R2 is consistent with the observed tendency, and is coinciding with horizontal axis. The correlation between the precursor content and the resonant frequency is qualitatively described by the growth of conductivity, which resulted in the frequency increasing.

The resonant interaction of another nature in the studied films is presented by Figure 4b, which shows the spectral curves $\rho(\lambda)$ for two samples in the extended wavelength range. One of them has an extremum at $\lambda \approx 950$ nm typical for the resonance effect; another due to the limited range, exhibits only a trend of increasing, which undoubtedly should lead to an extremum. The nature of these extrema will be identified by the corresponding spectral analysis. Figure 5 shows two curves $\rho(\lambda)$ re-plotted from the Figure 4 for samples T4.R0.5 and T4.R1, for the frequency dependences $\rho(\omega)$, i.e. to the form traditional for resonant phenomena. Furthermore, for clarity, they are normalized to the one and the same amplitude of the extremum. Both the characteristics are similar at the higher frequencies side relatively the resonant frequency $\omega_0=4.3\times10^{15}$ Hz, which indicates the general nature of the phenomenon in this frequency range. Since the samples were prepared with the same amount of the tin dioxide precursor, it is reasonable to associate the coincidence of the resonant frequencies with the coinciding number of centres interacting with light. Since the frequency range in Figure 5 is close to the saturation region of the dispersion dependence $\omega(k)$, describing the resonance phenomenon it can be concluded that the nature of that extremum is associated with local plasmon resonance on cluster particles.

However, curves *1* and *2* in Figure 5 are more complex than the elementary oscillator function, which is evidently asymmetrical relatively the resonant frequency ω_0, and, as a result, not coinciding with the normal distribution function (circles) in the region of frequencies lower than ω_0. These circumstances necessitated the approximation of them by two Gaussian functions, which is shown in Figure 6. It is evident that the approximation is so perfect that it allowed the determination of the key resonance parameters, i.e. the frequencies (ω_1, ω_2) and relaxation times (γ_1, γ_2). It is reasonable to apply this result obtained in the form of two components of the parameter $\rho(\omega)$ to two clusters' groups differing in sizes and shown in Figure 1. Supposing that the local plasmon energy relaxation time is controlled by scattering at the surface, it is reasonable to attribute the parameters $\omega_1=4.4\times10^{15}$ Hz, $\gamma_1=1.670^{-15}$ s and $\omega_2=4\times10^{15}$

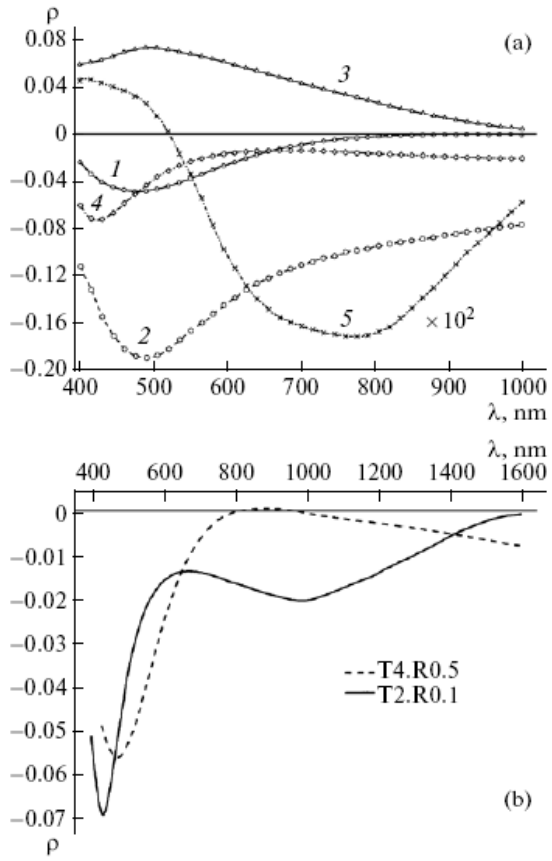

Figure 4: Spectral dependences of the polarization difference $\rho(\lambda)$ at an angle of incidence of 55°: (a) samples (*1*) T4.R0.5, (*2*) T4.R1, (*3*) T0.5.R0.1, (*4*) T2.R0.1, and (*5*) T2.R2; (b) for the samples T4.R1 and T4.R0.5 wavelength range is extended.

Hz, $\gamma_2=1.02\times10^{-15}$ s to clusters with increased and decreased sizes, respectively.

The same procedure was efficiently applied to the second, more complex dependence in Figure 5. The sample T4.R1, in addition to two components typical for the sample T4.R0.5, has one more resonant electromagnetic interaction in the studied frequency range i.e. excitation of the plasmon–polariton wave in the film, caused by the intercluster dipole–dipole interaction [17]. This interaction is illustrated in Figure 7 by an additional component, which being summed with two other Gaussian curves (the sum is the solid curve), is in good agreement with the experimental dependence (dots). The conditions of its appearance and the degree of its manifestation depend, in contrast to the local surface resonance, not only on the total number of interacting centres, but also on sizes, shape of clusters and the distance between them, which was suggested [18].

This fact is directly confirmed by the results of surface plasmon–polariton wave excitation, which is reflected both in the formation of a resonant extremum of the parameter $\rho(\omega)$ spectral characteristics for sample T2.R0.1 (Figure 4b) near the wavelength λ=980 nm, and in the tendency of the curve for sample T4.R0.5, which should develop as a resonant extremum with high probability. Exactly this resonance, which is spaced far from the local one in samples T4.R0.5

and T2.R0.1, comes closer to the local resonances at frequencies ω_1 and ω_2 in Figure 7 for the sample T4.R1, and has increased amplitude of the corresponding curve in Figure 4a.

Detailed reasons for the mentioned features in the spectral characteristics may be the subject of an independent study. Identification of the reasons may be facilitated by data on the parameters of local and polariton resonances. Such data are the resonant frequencies $\omega_1=4.38\times10^{15}$, $\omega_2=3.67\times10^{15}$, $\omega_3=2.3\times10^{15}$ Hz, and the oscillation relaxation times $\gamma_1=1\times10^{-15}$, $\gamma_2=0.71\times10^{-15}$, $\gamma_3=0.48\times10^{-15}$ s obtained for three components from the Gaussian functions (Figure 7).

The most notable illustration of the connection between the parameter ρ spectral characteristic peculiarities and the film morphology was obtained in the second type samples studies. In their case the resonance's positions were distributed along the frequency axe. Figure 8 gives the spectral characteristics of the polarization

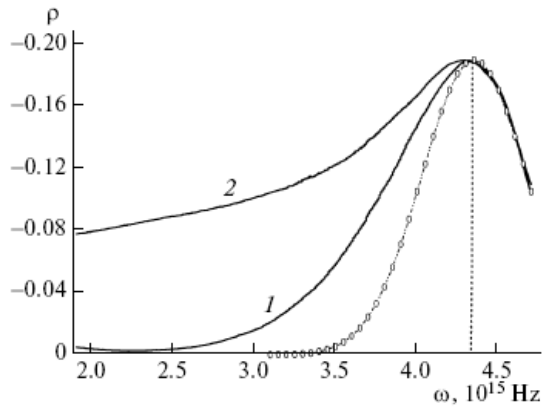

Figure 5: Frequency dependences of parameter ρ for samples (*1*) T4.R0.5 and (*2*) T4.R1, recalculated from the data of Figure 4a and normalized to the extremum, in comparison with the normal Gaussian distribution function (circles).

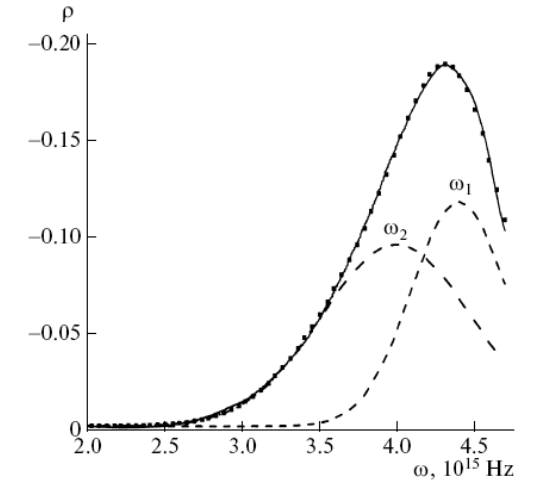

Figure 6: Frequency dependence of the parameter ρ for the sample T4.R0.5 (dots), recalculated from the corresponding dependence ρ(λ) (Figure 4a), in comparison with the normal Gaussian distribution function (solid curve) expanded in two components (dashed curves).

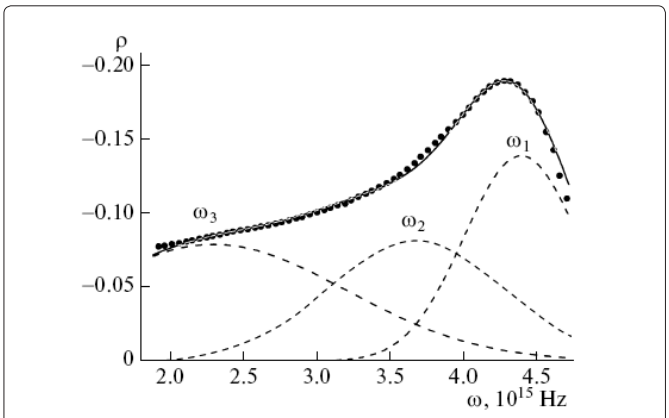

Figure 7: Frequency dependence of parameter ρ for sample T4.R1 (dots), recalculated from the corresponding dependence ρ(λ) (Figure 4a), in comparison with the Gaussian distribution function (solid curve) expanded in three components (dashed curves).

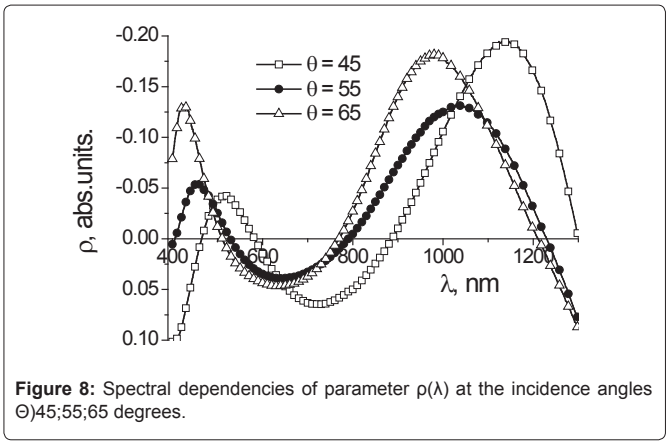

Figure 8: Spectral dependencies of parameter ρ(λ) at the incidence angles Θ)45;55;65 degrees.

difference for three angles' values of radiation incidence in the usual for resonance phenomena presentation. Their negative values are depicted in the upper part of coordinates. The parameter ρ negative sign also witnesses the resonance nature of light interaction with the clustered films. Hence, it may be concluded that these extrema in each of the three dependencies reflect the resonance character of radiation interaction with a film, more over, for both s-and p-states of polarization. At the same time, the resonance features both in the initial characteristics $R^2_s(\lambda)$ and $R^2_p(\lambda)$, and for the angular dependencies, are present in the reduced amplitudes of reflection coefficients. But in such a presentation, the resonances are not clear.

But, nevertheless, the differences of amplitudes and shapes of dependencies are manifested clearly in the characteristic of difference, which is a ρ parameter. Two extrema in the spectral dependencies registered at one and the same angle of incidence are due to the resonance excitation. Their nature is usually connected with local SPR at short waves length for radiation (420, 455, 516 nm), and polariton resonance at longer waves lengths (λ=976, 1034, 1140 nm). Such a split of the SPR may be attributed both to the simple composition of films, but with a percolation structure, and to composite type films, which contain metal clusters in the dielectric matrix [19].

In such a case, the unusual may be the fact, that firstly, the resonance wave length (frequency) dependence on the radiation

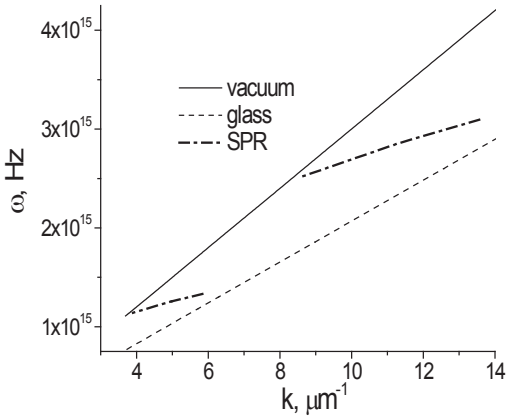

Figure 9: The dispersive characteristics of surface plazmons in the film (dot and dash) lines, light characteristics in vacuum (solid line) and in glass (dash line).

incidence angle is observed not only for the polariton, but also for local SPR.

Secondly, the SPR split value exceeds the half width of each of the resonances. Moreover, it increases with the angle decrease, resembling the behavior for forbidden photon zone, which is specific to the regular structures [20].

But, as it follows from the phase AFM topology, the films consist of slightly contacting clusters, with their shapes projected on a plane as circles. Additionally, both a little part of normalized, according to Singh and Gupta [11], resonance energy transfer and disordered clusters' location, irrespectively to their little spread of sizes gives no basis for the conclusion about the photons' nature of spectral characteristics.

In such a case, the single understanding of resonances' nature may be obtained from dispersion characteristics ω(k), presented at Figure 9. As it appeared, both the excitations are specific for polariton waves, which have practically equal group velocities. The fact that they have different frequencies may be connected with Plasmon's' frequency dependence [21] on particles sizes. In our case, the particles' cross section coinciding with a field wave direction, which is dependent on the incidence angle may play a role of such a size.

Hence, the mentioned peculiarities are reasonable to attribute to the clusters nonsphericity, which due to the technology of their preparation have ellipsoidal shape. The clusters were mainly oriented in the direction of their growth, which causes the films' dielectric properties anisotropy.

The additional confirmation of such a conclusion is supported by Lozovski et al. [22], where such property was simulated by transmission calculations. Its value is crucially dependent on the field wave azimuth relatively to a dipole axe.

The direct use of this calculation result has a limitation, due to its proximity, but qualitative matching of the results in the form of ρ parameter dependence on the orientation is fully acceptable.

Conclusions

The general principles of the SPR phenomenon [3] are consistent with its existence in tin dioxide films. This conclusion excepting the work [23], was not widely discussed in publications.

The validity of such studies is proved by reasons mentioned in the Introduction, and also by the observed strong parameter ρ response to the changes both in the films' optical properties, and to external medium parameters. Such films' properties may have both material applications and in physical theory.

Realisation of such physical parameters requires corresponding physical equipment and technological support in fabrication films with reproducible parameters.

The principal physical results obtained in the study show that the polarization difference negative sign (anomalous reflection) $\rho=R_s^2-R_p^2$ witnesses the metal nature of light absorption in films. However, as it was shown previously [8], the interval of negative ρ and the shape of its angular dependence differ significantly for continuous and cluster films. For example, its increased extension in the region of angles larger than the critical one is exclusively associated with a structure of clusters. This fact, confirmed by independent studies, may be a basis for its application as a diagnostic tool.

The confirmation of the obtained results makes it possible to solve the most important problem of composite nanomaterials, i.e. determination of cluster shape. The necessary data may be obtained from the relations for $R_{S|SP}^2$ and $R_{P|SP}^2$, characterizing the degree of resonant interaction, and the angular and spectral dependences of the parameter ρ.

The used spectral analysis technique makes it possible to obtain information on the physical nature of resonances, their frequency and relaxation parameters, and the related structural and crystalline perfection of samples.

References

1. Batzill M, Diebold U (2005) The surface and materials science of tin oxide. Prog Surf Sci 79: 47-154.
2. Agranovich VM, Mills DL (1982) Surface Polaritons: Electromagnetic waves at surfaces and interfaces. North-Holland Pub. Co., Elsevier Science Ltd., Amsterdam, Moscow.
3. Dmitruk NL, Litovchenko VG, Strizhevskii VL (1989) Surface polaritons in semiconductors and dielectrics. Nauk Dumka Kiev.
4. Otto A (1968) Excitation of nonradiative surface plasma waves in silver by the method of frustrated total reflection. Z Phys 216: 398-410.
5. Kretschman E (1971) The determination of the optical constants of metals by excitation of surface plasmons. Z Phys 241: 313-324.
6. Berezhinskii LI, Maksimenko LS, Matyash IE, Rudenko SP, Serdega BK (2008) Polarization modulation spectroscopy of surface plasmon resonance. Opt Spectrosc 105: 257-264.
7. Jasperson SN, Schnatterly SE (1969) An improved method of high reflectivity ellipsometry based on a new polarization modulation technique. Rev Sci Instrum 40: 761-767.
8. Berezhinskii LI, Litvin OS, Maksimenko LS, Matyash IE, Rudenko SP, et al. (2009) Size effects in the internal reflection in gold cluster films in polarization modulation experiments. Opt Spectrosc 107: 264-269.
9. Born M, Wolf E (1999) Principles of optics. Cambridge University Press, Cambridge, UK.
10. Vinogradov EA, Leskova EA, Ryabov AP (1994) Opt Spectrosc 76: 282.
11. Singh S, Gupta BD (2010) Simulation of a surface plasmon resonance-based fiber-optic sensor for gas sensing in visible range using films of nanocomposites. Meas Sci Technol 21: 115202.
12. Filevskaya LN, Smyntyna VA, Grinevich VS (2006) Morphology

of anostructured SnO_2 films prepared with polymers employment. Photoelectronics, Astropint, Odessa 15: 11-14.

13. Ulug B, Turkdemir HM, Ulug A, Buyukgungor O, Yucel MB, et al. (2010) Structure, spectroscopic and thermal characterization of bis(acetylacetonato) dichlorotin(IV) synthesized in aqueous solution. Ukr Chem J **7:** 12-17.
14. Miloslavskiy VK (1959) Opt Spectrosc 7: 244.
15. Azzam RMA, Bashara NMI (1989) Ellipsometry and polarized light. North Holland, New York, USA.
16. Anastasescu M, Gartner M, Mihaiu S, Anastasescu C, Purica M, et al. (2006) Optical and structural properties of SnO2-based sol-gel thin films. Proceedings of the IEEE International Semiconductor Conference 1: 163-166.
17. Evlyukhin AB (2005) Scattering cross-section of surface plasmon polaritons nanoparticle in the dipole approximation. JTP Lett 31: 14-21.
18. Shalin AS, Moiseev SG (2009) Optical properties of nanostructured layers on the surface of an underlying medium. Opt Spectrosc 106: 916-925.
19. Grynko DA, Barabash YM, Maksimenko LS, Matyash IE, Mishchuk ON, et al. (2012) Modulation polarimetry of the topological effect in gold-organic nanocomposite films. Physics of the Solid State 54: 2301-2308.
20. Gippius NA, Tikhodeev SG, Christ A, Kuhl J, Giessen H (2005) Waveguide plasmon polaritons in metal-dielectric photonic crystal slabs. Physics of the Solid State 47**:** 145.
21. Kreibig U, Vollmer M (1995) Optical properties of metal clusters. springer series in materials science. Springer-Verlag, Berlin, Germany.
22. Lozovski V, Schrader S, Tsykhonya A (2009) Possibility of surface plasmon-polaritons amplification by direct current in two-interface systems with 2D Bragg structure on the surface. Opt Commun 282: 3257-3265.
23. Serdega BK, Matyash IE, Maximenko LS, Rudenko SP, Smyntyna VA, et al. (2011) Optical constants detection in tin dioxide nano-size layers by surface plasmon resonance investigation. Semiconductors 45: 316-319.

Author Affiliations

Top

[1]*Odessa Mechnikov National University, ul. Dvoryanskaya 2, Odessa, 65082, Ukraine*
[2]*Lashkaryov Institute of Semiconductor Physics, National Academy of Sciences, pr. Nauki 41, Kyiv, 03028, Ukraine*